ROTOR DYNAMICS MODIFICATION OF AN EIGHT STAGE COMPRESSOR FOR SAFETY/RELIABILITY IMPROVEMENT

by

Francis H. Kludt

Staff Rotating Equipment Engineer

Celanese Chemical Company

Pampa, Texas

and

Dana J. Salamone

Chief Engineer

Centritech Corporation

Houston, Texas

Francis H. Kludt received his B.S. degree in Mechanical Engineering from Texas A&M University in 1969. He is the Staff Rotating Equipment Engineer for the Celanese Chemical Company at their Pampa, Texas plant. He has prior experience with Olin Corporation and with Westinghouse Electric Corporation. While with Olin, at their Lake Charles, Louisiana plant, Mr. Kludt's responsibilities included the rotating equipment in the ammonia plant and in the complex. His experience with Westinghouse Electric included field service on mechanical drive/power generation steam turbines, maintenance contracts, quality assurance for steam turbine manufacture, supplier qualifications, field installation and retrofit programs.

He is a member of ASME and the Vibration Institute.

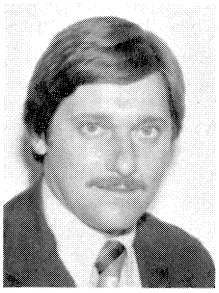

Dana J. Salamone is Chief Engineer for Centritech Corporation in Houston, Texas. In this capacity, he is a bearing designer and consultant to the utility, petroleum and chemical industries for the solution of turbomachinery vibration problems. He has nine years of industrial experience in stress analysis, structural vibrations, and rotor dynamics. Mr. Salamone earned his B.S. degree in Mechanical Engineering in 1974, and his M.S. degree in Applied Mechanics in 1977, both from the University of Virginia. He is a member of ASME and has authored several ASME publications in the area of rotor dynamics. He is also a registered professional engineer in the State of Texas.

ABSTRACT

The catastrophic failure of a high pressure centrifugal air compressor utilizing air-pressurized bearing housings dictated the redesign of its sister compressor. The modification of this early 1950's compressor involved elements of both practical and analytical design. The project included the design of new bearings and seals and the alteration of various support systems to permit operation with non-pressurized bearing housings.

The project was undertaken as risk minimization, with all performance and reliability improvements being additional benefits. The matching of the computer model with the field data of the existing system was the key to its successful evaluation. It was found that a case seal was acting as an additional bearing during certain operating conditions. This third bearing caused the compressor to behave differently than had been predicted with the initial two-bearing models. With the system properly modeled, changes were proposed to optimize the rotor dynamics. The main objectives were to achieve reliable rotor dynamic characteristics and to maintain the integrity of the process labyrinth seals.

The changes were made in April, 1982, with the normal hardware fitting considerations. The subsequent start-up and operation were without incident. The modified compressor has performed well through a number of emergency trips and subsequent restarts, exhibiting exceptional rotor stability and overall reliability.

INTRODUCTION

The utilities section of the Celanese Pampa Plant uses two high pressure stage centrifugal compressors (see Figures 1 through 4) to compress air to 800 psi. Until recently, these units had operated with pressurized bearing housings similar to those found in refrigeration compressors. These high stage compressors operated without major problems for about 28 years. Then, in 1980, an incident involving an unusual set of circumstances led to the destruction of one of the compressors. A subsequent investigation indicated that oil from the bearing housing had been ingested into the compressor while it was in heavy surge. This had led to an internal explosion, which damaged the compressor beyond repair. A replacement compressor of a different design was subsequently purchased and installed.

These high pressure compressors were designed to compress air from 260 psi to 800 psi in eight diaphragm-cooled stages. The bearing housings were pressurized with air at about 15-20 psi below suction pressure via pressure regulators. This differential pressure control limited the leakage across the process labyrinth seals. Figure 5 schematically illustrates the compressor system. The compressor was driven by a 3,500 horsepower steam turbine to a maximum operating speed of 10,000 rpm, using a gear-type coupling.

After the incident, it was necessary to address the problem of how to deal with the remaining sister compressor, which still employed the pressurized bearing housings. In spite of the fact that the circumstances surrounding the original failure were very unusual, and that their combination on that particular day was a first time occurrence, there was nothing to

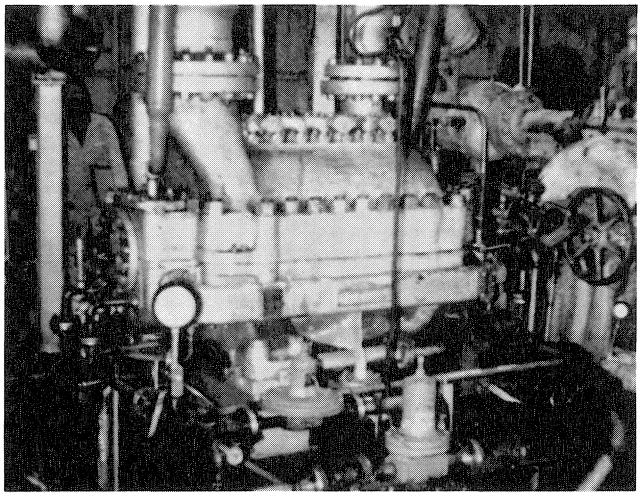

Figure 1. Assembled Case With Control and Lube Piping.

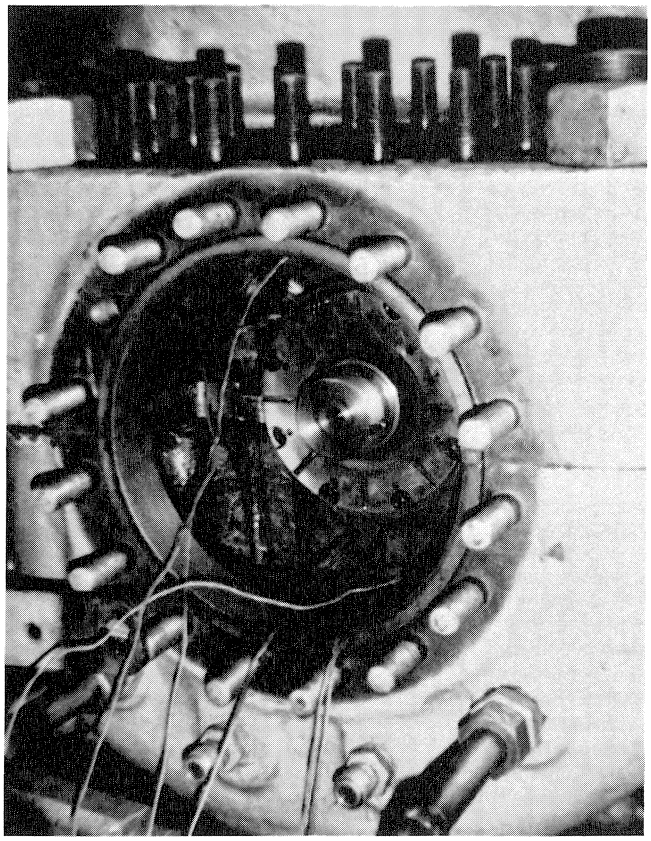

Figure 2. Thrust End Bearing Housing.

prevent them from occurring on the other unit.

The plant decision was to either modify the existing compressor to prevent the possibility of oil ingestion or to replace the compressor with a new design. Since the estimated cost of a new compressor installation was in excess of one million dollars, there was sufficient incentive to investigate the alternative of modifying the existing compressor.

MAINTENANCE HISTORY

The turbine, compressor, and process require trips and interlocks which will shut down the turbine in the event of a process upset. These units were relatively simple to restart

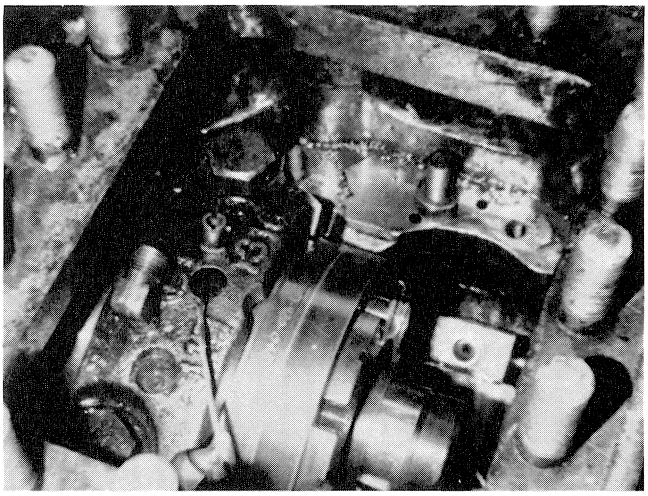

Figure 3. Top View of Thrust Housing Showing Space Limitations.

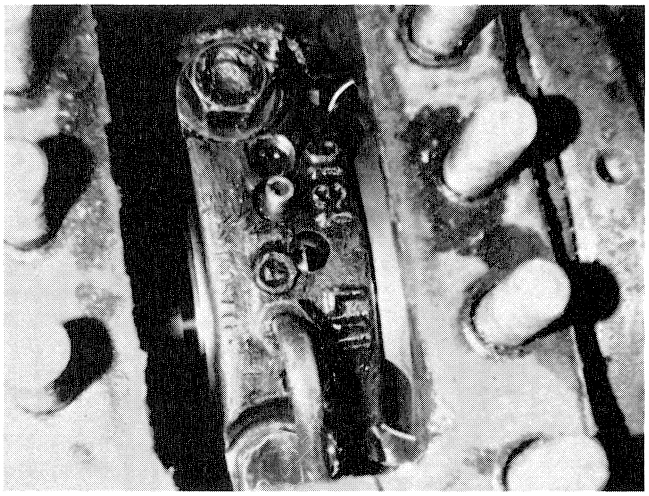

Figure 4. Top View of Discharge End Bearing Housing Showing Space Limitations.

after they had tripped. However, the compressors did accumulate a considerable maintenance history. The early model vibration instrumentation installed on the compressor was usually functional, but it was not trusted, primarily due to its computer interface. Measured case data, acquired with hand-held instruments, were more readily accepted.

The compressor was generally predictable, and the plant personnel were successful in meeting its maintenance requirements. Process seal and bearing replacement was a routine job. With regard to the process labyrinth seals, a change from the original brass material to nickel silver increased the shaft life and, therefore, increased the interval between major overhauls. Four conclusions could be drawn from the maintenance history:

1. Most of the maintenance problems encountered with the compressor were associated with start-ups and shutdowns. The bearings and process labyrinth seals were good for about two trip-outs and restarts, before the seal leakage exceeded the amount for which the regulators could compensate while still maintaining the bearing housing pressure differential. It was suspected that there were significant shaft excursions, which caused seal damage, during these transient periods.

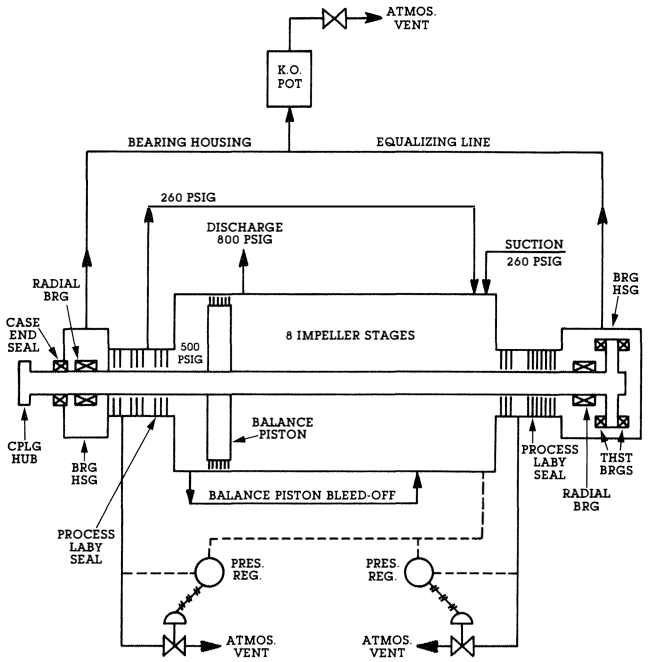

Figure 5. Compressor System Schematic.

2. The rotor was very sensitive to coupling unbalance. This was evidenced when the inadvertent installation of an undersized coupling key caused case vibration in excess of 1.0 in/sec.
3. Surges or other abnormal operation would cause further seal and bearing damage that usually necessitated a major overhaul.
4. Although these problems were not unusual, long periods of successful operation were common.

HISTORICAL VIBRATION DATA—ORIGINAL SYSTEM

The compressor displayed evidence of occasional significant shaft excursions by wiping the process labyrinth seals enough to indicate as much as 0.017 in. radial movement. It is important to note that the end of the seal cartridge was only 1.0 in. from the journal bearing, which had a radial clearance of only 0.003 in.

The high case velocities that resulted from the installation of an undersized key in the drive coupling made us keenly aware of the rotor's sensitivity to unbalance in that location. In addition, it was observed that the compressor was sensitive to the rate of speed change, load change and surge conditions. Therefore, it routinely required careful handling. In fact, most seal and bearing failures occurred during start-ups and shutdowns. It was also noted that the vibration spectra from starts and stops were not repeatable in terms of amplitudes and secondary vibration frequencies. Table 1 contains some typical vibration data measured during normal operation.

PRACTICAL PROBLEM ANALYSIS—ORIGINAL SYSTEM

Management Guidance

Plant management required that if there was not absolute certainty that the modification would perform as predicted on the first start-up, the compressor would have to be replaced with a new unit.

Table 1. Typical Field Data During Normal Operation.

LOCATION	SHAFT PROXIMITY PROBES		CASE VELOCITY (IN/SEC)
	FILTERED FREQUENCY (CPM)	AMPLITUDE (MILS)	
SUCTION END	ALL PASS	1.3	0.13 - 0.15
	9,200	0.76	
	7,250	0.37	
	14,400	0.16	
	18,350	0.35	
DISCHARGE END	ALL PASS	0.8	0.18 - 0.25
	7,300	0.35	
	9,200	0.35	
	14,400	0.14	
	18,500	0.08	

NOTE: MINOR VIBRATION PEAKS TYPICALLY SEEN AT 3,150, 4,200, 5,775 AND 6,300 CPM WERE NOTED AT OTHER TIMES.

Confusion Factors

The compressor manufacturer was approached for suggestions. They stated that their case design had been changed many years ago to eliminate the pressurized bearing housings, and they would not attempt a conversion of the existing case to atmospheric pressure bearing housings for the following reasons:

1. Excessive leakage to the atmosphere would result.
2. Inadequate internal case porting would result in high thrust loads.
3. Case and spacing problems would result in either pressurized bearing housings or extreme oil vapor blow off.
4. The case casting variations might preclude modification.

They recommended the purchase of a new compressor.

Prior to Centritech's involvement, a contract engineering house did a study on this compressor. They felt that it could be easily modified to an atmospheric bearing housing and proposed a design. However, their analysis of the existing system did not inspire confidence, since it did not match the physical evidence (because of too many assumptions). Also, their seal analysis was felt to be overly simplistic.

Vibration Analysis Data

The unpredictable rotor vibration characteristics caused several weekends of unscheduled maintenance. In addition, the indicated amplitude of movement (but not the measured amplitude) caused us to question the placement of our vibration probes. It was interesting to note that the vibration on the outboard end of the compressor had about the same amplitude as that of the inboard end during our coupling unbalance study. The apparent proximity of the operating speed to the second critical speed was of concern. The presence of some inconsistent peaks at approximately half frequency (on the outboard end), and cross-talk from the turbine (on the inboard end) also caused concern. It was felt that the key to successful operation would be to eliminate these high amplitude shaft excursions in order to avoid subsequent seal damage. Figures 6 through 10 contain field data measured on the compressor before any alterations.

Figure 6 shows peak hold probe amplitudes taken during a shutdown. Note the high discharge (coupling) end amplitude resulting from the half-key unbalance condition. Also, note the influence of this excitation on the suction end. During the time

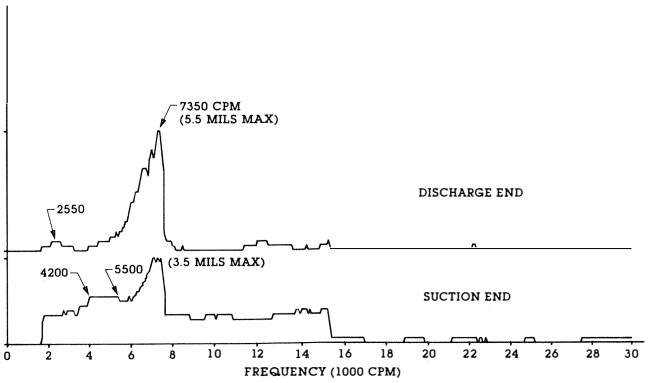

Figure 6. Pre-Conversion Peak Hold Probe Amplitudes (9/18/80 Shutdown).

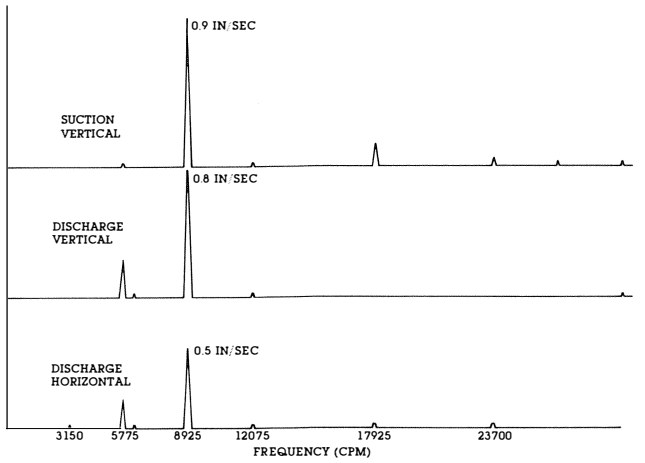

Figure 7. Pre-Conversion Case Velocity Spectrum (8/21/80).

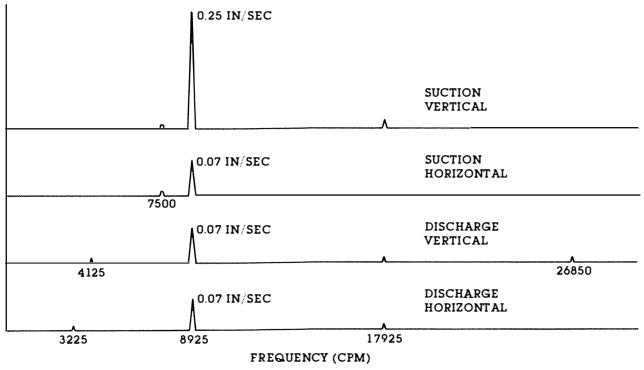

Figure 8. Pre-Conversion Case Velocity Spectrum (10/20/80).

when the Figure 7 data were taken, the overall case vibration was 1.0 in/sec. Figure 8 is a case velocity spectrum showing the vibration after the correction of the coupling key unbalance, noted in Figures 6 and 7. Note, in particular, that the relationship between the suction and discharge amplitudes has changed. The suction end vibration became predominant with the correction of the coupling unbalance. Figures 9 and 10 are waterfall diagrams taken during a start-up, after correction of the coupling key unbalance problem. These results also indicate the high suction end vibration.

Physical Measurements of Process Labyrinth Seals

The original process labyrinth seals typically showed a 10

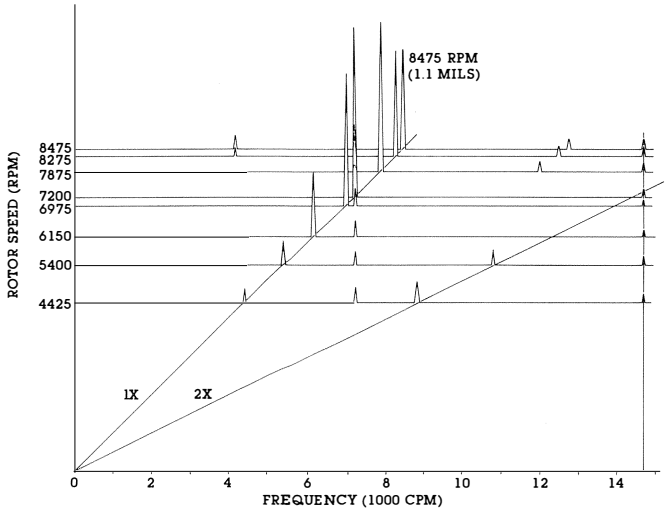

Figure 9. Pre-Conversion Waterfall Diagram—Discharge End (10/18/80 Start-Up).

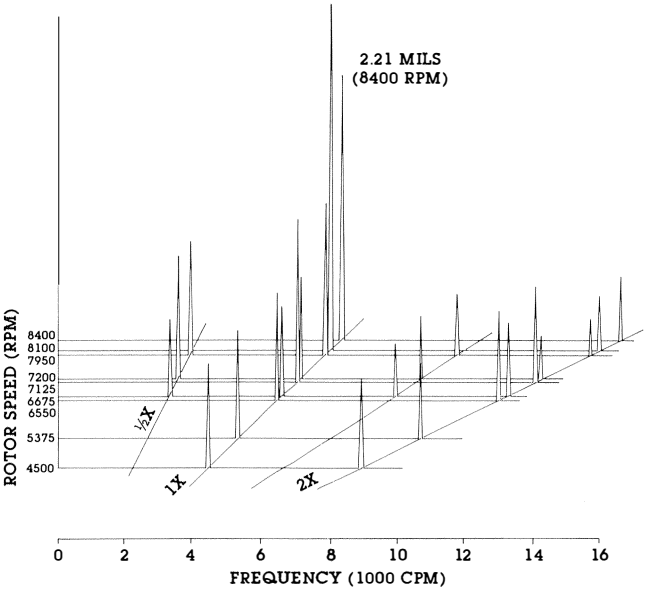

Figure 10. Pre-Conversion Waterfall Diagram—Suction End (10/18/80 Start-Up).

to 32 mil increase in diameter when removed from service due to excessive leakage. The damage was due to shaft contact on the labyrinth seal teeth. There was approximately the same amount of damage on both ends of the suction end seal. However, on the discharge end seal, there was significantly more damage on the inboard end than on the outboard end. Figure 11 illustrates the original seal. Table 2 lists typical seal measurements before and after service.

Shaft Transient Vibration Concern

It was felt that shaft excursions during transient periods were responsible for our seal problems. Since part of the new design involved increasing the pressure drop across the same seal length, the control of these seal clearances during transient periods was absolutely essential. Therefore, it was required that the dynamic response analysis match the physical evidence, in order to ensure that the system was properly modeled. If this match could be accomplished, a plan could be developed to alleviate the problems.

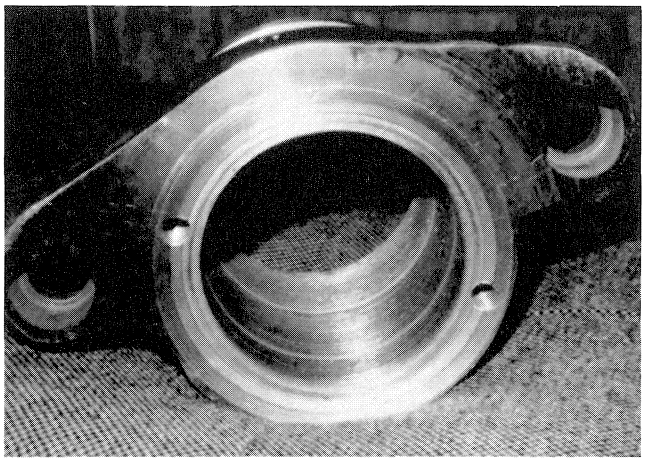

Figure 11. Original Process Labyrinth Seal.

Table 2. Physical Measurements—Original Process Labyrinth Seals.

NEW SEAL DIAMETER 3.508 INCHES

USED SEAL DIAMETERS (INCHES):

SUCTION END

	OUTBOARD	INBOARD
VERTICAL	3.530	3.538
HORIZONTAL	3.530	3.536

DISCHARGE END

	OUTBOARD	INBOARD
VERTICAL	3.516	3.540
HORIZONTAL	3.508	3.520

Maintenance Requirements

It was required that any proposed solution should necessitate less frequent maintenance than the existing system. In addition, the new system had to be practical. In other words, the average mechanic should be able to assemble and disassemble it without special training and with a minimum of special tools.

Process/Financial

In addition to the usual process demands for reliable normal operation, the system must withstand trips, start-ups and mild surges without requiring unscheduled maintenance and incurring the cost of lost production. These criteria were met by the new compressor that had replaced the failed unit. Therefore, it was expected that the modified sister compressor meet these same requirements. If these expectations could not be met, a new unit would be purchased as the replacement (at a very high cost).

Practically speaking, it appears to be more acceptable to buy a proven piece of new equipment than to perform an unproven modification on an old one. With new equipment purchases, it seems to be easier to obtain funds: fewer questions are asked, the scenario is easily understood, fewer detailed explanations are required, and there appear to be fewer unexpected complications. Therefore, the potential risks of modification had to be carefully weighed against the high cost of replacement.

ROTOR DYNAMICS ANALYSIS

Centritech Corporation was contracted to perform a rotor dynamic analysis and bearing optimization study on this eight stage centrifugal air compressor. The original rotor system consisted of a 402 lb rotor with a 45.5 in. bearing span. The rotor was supported by two 2.5 in. diameter pressure dam journal bearings. There was a floating ring oil seal on the coupling end bearing housing to seal the case penetration at the driven end. This seal required an oil supply of about 290 psi.

Computer Model

The compressor rotor cross section shown in Figure 12A is modeled as a series of lumped mass stations containing the weight and inertia properties of the compressor wheels, balance piston, coupling, thrust collar, etc. These mass stations are mathematically interconnected by elastic shaft elements. The rotor model also contains the bearing support locations, with the speed-dependent stiffness and damping properties of the oil film. Figure 12B shows the computer model indicating division of the rotor shaft into discrete sections for modeling. Each section line indicates a mass station.

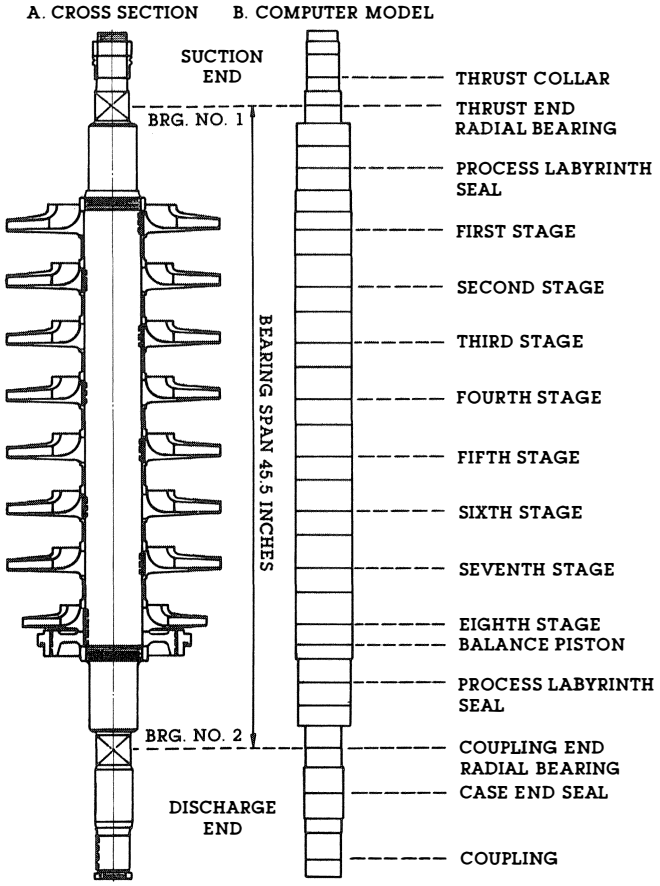

Figure 12. Compressor Rotor.

Undamped Critical Speeds

The critical speed map for the original rotor is shown in Figure 13. The first critical speed (first mode) has a rigid bearing limit of 5,730 rpm. Therefore, the shaft stiffness is 1.87×10^5 lb/in. This is a very flexible rotor, as indicated by the "flatness" of the first mode curve.

The rotor mode shapes indicate the relative rotor amplitudes at the undamped critical speeds. Figures 14 through 16 are undamped critical speed mode shapes for the existing

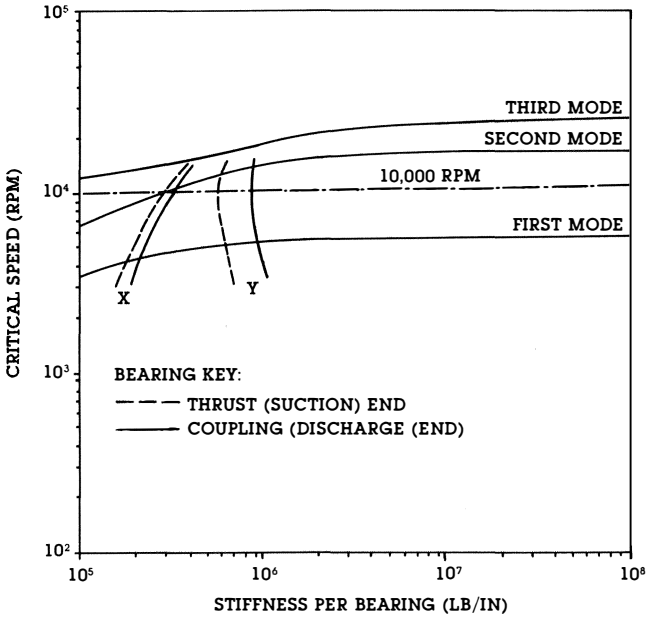

Figure 13. Critical Speed Map With Original Bearing Stiffness.

rotor, considering arbitrary bearing stiffnesses of 1×10^5, 5×10^5, and 1×10^7 lb/in. Note that Figure 14 shows only moderate rotor bending, because a bearing stiffness of 1×10^5 lb/in is quite flexible for this shaft. The first and second modes for this bearing stiffness are cylindrical and conical, respectively. If the bearing stiffnesses were increased to 5×10^5 lb/in (Figure 15), there would be considerably more rotor bending than for the previous case. There is still some motion at the bearings to provide damping forces. Therefore, the bearings appear stiffer relative to the shaft, but they are not yet rigid. Finally, if the bearing stiffnesses were increased further to 1×10^7 lb/in (Figure 16), there would be no bearing motion. This represents the rigid bearing case, in which the bearings have become far too stiff for the rotor and contribute no effective damping. Referring to the critical speed map (Figure 13), this condition would occur at bearing stiffnesses above 2×10^6 lb/in. Therefore, an alternate bearing design must not exceed this bearing stiffness value at the first critical speed, in order to allow safe operation through this mode.

Another interesting observation is the unusual second mode shape for a bearing stiffness of 5×10^5 lb/in in Figure 15. At this stiffness value, there is almost zero relative amplitude from the suction (thrust) end to the middle of the shaft, but there are large relative amplitudes at the coupling end. Therefore, at these stiffnesses, the thrust end journal bearing has very little motion to provide damping to the rotor.

Original Pressure Dam Bearings

The original bearings, shown schematically in Figure 17, are pressure dam bearings. Both ends are identical, with diameters of 2.5 in., widths of 1.8 in., dam widths of 0.875 in., and relief track widths of 0.81 in. The dam angles are 135 degrees from the split line, in the direction of rotation. The specified diametral running clearance ranges are 0.0045 to 0.0060 in., and the dam step heights are approximately 0.032 in. Therefore, the dam depth-to-clearance (radial) ratio is approximately 15. This is very high, compared to recommended values of 3 to 6 [1].

The lubricating oil utilized was rated at 218 ssu at 100°F. Therefore, its absolute viscosity was 1.98×10^{-6} reyns (lb-sec/in^2) at 150°F.

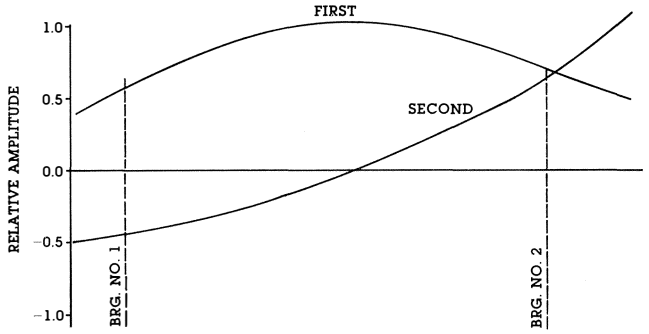

Figure 14. Mode Shapes for Bearing Stiffness = 1×10^5 lb/in.

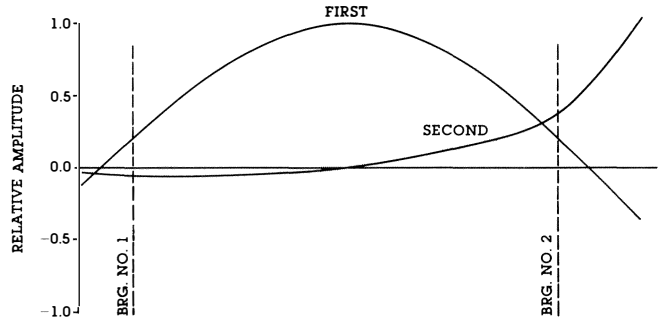

Figure 15. Mode Shapes for Bearing Stiffness = 5×10^5 lb/in.

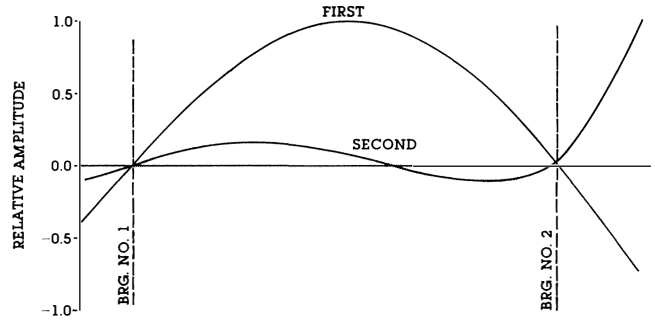

Figure 16. Mode Shapes for Bearing Stiffness = 1×10^7 lb/in.

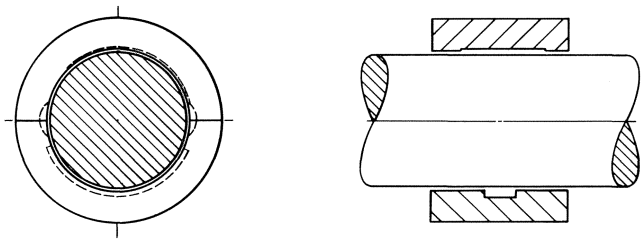

Figure 17. Original Pressure Dam Bearing.

Table 3. Undamped Critical Speeds With Original Pressure Dam Bearings.

	HORIZONTAL PLANE	VERTICAL PLANE
FIRST CRITICAL	4,200 - 4,350 RPM	5,150 - 5,300 RPM
SECOND CRITICAL	10,000 - 10,500 RPM	12,500 - 14,000 RPM
THIRD CRITICAL	ABOVE 15,000 RPM	ABOVE 15,000 RPM

The principal stiffness and damping coefficients are shown on the original critical speed map (Figure 13). Table 3 lists the undamped critical speeds. Note that the second horizontal critical is very close to the maximum operating speed.

Case End Seal

Figure 18 illustrates the floating ring case end seal, which consists of two floating bushings (shown with "L" shaped cross sections). The inboard side of this seal is exposed to approximately 250 psig air, which is in the bearing housing. The outboard side is at atmospheric pressure. High pressure oil, at 290 psig, is supplied between the two bushings to provide an oil barrier against bearing housing leakage. Oil leakage out the inboard side bushings flows into the bearing housing. Oil leakage out the outboard side bushing is partially captured in the drain groove at the end of the bushing. Oil passing along the shaft is stopped by the oil slinger ring and exits out the drain.

A complete simulation of this oil seal configuration would require a very complex non-linear analysis. However, with a few simplifying assumptions, the seal effect can be approximated in order to assess the influence on the system dynamics. Specifically, a calculation of the unbalanced pressure forces on the floating bushings can be made. These forces then can be used to estimate the order of magnitude of the friction force on the sliding faces. It should be emphasized that this is a simplistic approximation and that the actual seal exhibits a combination of hydrodynamic bearing and sliding friction behavior. This analysis assumes two boundary conditions for the seal effect.

Figure 19A shows that the inboard bushing is exposed to 250 psig air pressure on the inboard face and 290 psig oil on the other faces. Therefore, the net unbalance pressure differential is 40 psig. The unbalanced region and the pressure differential for this bushing are small, compared to those of the outboard bushing. Therefore, the effect of the inboard bushing was neglected in the model.

The outboard bushing, shown in Figure 19B, is exposed to 290 psig oil on the free face. On the sliding face, there is an O-ring to seal leakage from getting behind the bushing. Above this O-ring is 290 psig oil, and below is about 20 psig bearing housing seal drain pressure. This provides an axial pressure differential of approximately 270 psig on the bushing. The unbalanced region between the O-ring and the bore has an area of approximately 4.92 in^2. Therefore, the net force between this bushing and the support housing is 1,300 lb. If we assume hard steel-on-hard steel (greasy), the static friction coefficient is 0.11. This would yield a static friction force of approximately 140 lb.

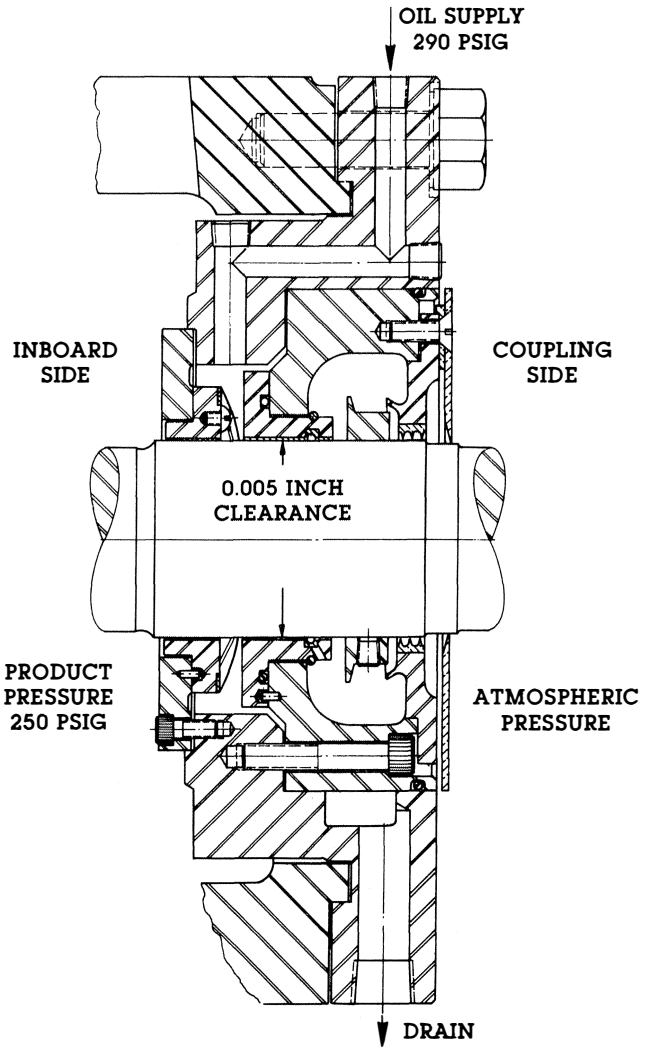

Figure 18. Case End Seal.

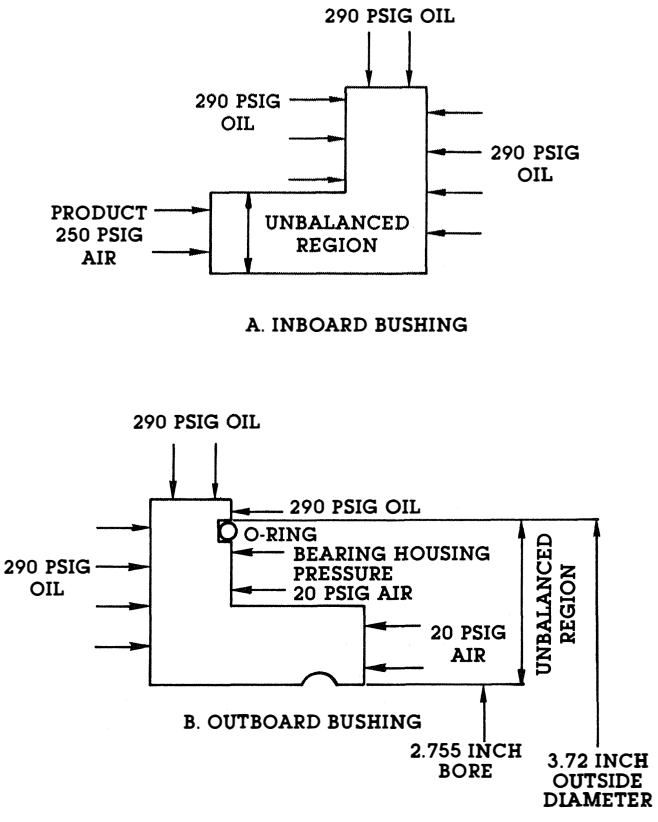

Figure 19. Case End Seal Bushings.

Figure 20 is a load versus eccentricity curve for the outboard bushing operating at a speed of 10,000 rpm and at an average external pressure of 155 psi. Figure 19B illustrates the pressure breakdown for 290 to 20 psig. Note that the bushing diametral clearance is 0.005 in. Therefore, if the friction force were large enough to lock this seal, it would act very much like a plain journal bearing with external pressurization. The load/eccentricity figure indicates the static friction line, showing the load at which the hydrodynamic capacity equals the approximated static friction force at the bushing-to-housing interface. From a static point of view, the bushing is not capable of generating more load capacity than can be held by this friction force. This means that the load/eccentricity curve ends at the 140 lb line for this approximation. At loads above this static friction line, the seal would slide, because the friction force would be exceeded. Consequently, the seal would move to a new position. Note that the intersection between the static friction line and the maximum operating speed line (10,000 rpm) is at an eccentricity of 0.27. This would be the eccentricity of the bushing, relative to the shaft.

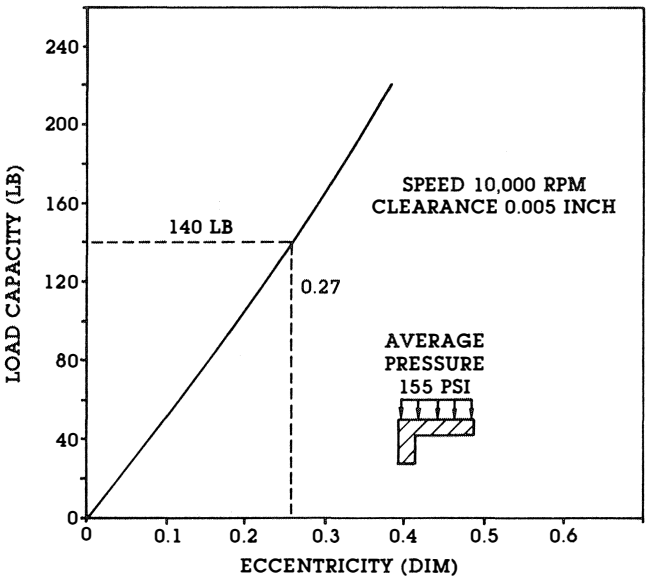

Figure 20. Seal Bushing—Load Versus Eccentricity.

Table 4 is a tabulation of the stiffness and damping coefficients versus operating speed for the case end seal bushing previously described. The bushing journal is 2.75 in. in diameter, and the length-to-diameter ratio is 0.32. This table also lists the eccentricity versus speed, and the stability condition of this bushing as a plain journal bearing. Note that the bushing is an unstable bearing for speeds of 3,000 rpm and above. Therefore, when the bushing seal is locked, it contributes high cross-coupling, which leads to a destabilizing effect on the rotor. In addition, the principal stiffness and damping would introduce the effect of a flexible third bearing into the overall system dynamics.

Two opposite extreme conditions were assumed to assess the case end seal effects. Recall that an eccentricity of 0.27 corresponds to the condition that the hydrodynamic load equals the assumed static friction load of 140 lb. Case One assumes that the seal is on top of the shaft and locked, with a relative eccentricity of 0.27. Case Two assumes that the seal is under the shaft (sharing the bearing load), with a relative eccentricity of 0.27. Therefore, in Case One, the seal exerts a 140 lb force "down" on the shaft, and in Case Two, the seal exerts a 140 lb force "up" on the shaft. These seal forces are

Table 4. Stiffness and Damping Coefficients for Locked Case End Seal.

	SPEED (RPM)			
	1000	3000	5000	10000
STIFFNESS (LB/IN)				
KXX	2.084×10^5	-7.09×10^2	$+4.72 \times 10^2$	$+1.31 \times 10^3$
KXY	$+4.44 \times 10^4$	$+9.547 \times 10^4$	$+1.245 \times 10^5$	$+2.084 \times 10^5$
KYX	-3.39×10^5	-2.239×10^5	-2.073×10^5	-2.517×10^5
KYY	4.077×10^4	3.836×10^3	2.771×10^3	2.042×10^3
DAMPING (LB-SEC/IN)				
CXX	6.897×10^3	1.534×10^3	8.126×10^2	4.634×10^2
CXY	-1.192×10^3	-1.589×10^1	-4.52	-0.54
CYX	-1.276×10^3	-1.589×10^1	-4.52	-0.54
CYY	1.385×10^3	6.066×10^2	4.745×10^2	3.973×10^2
ECCENTRICITY	.81	.59	.45	.27
STABILITY	STABLE	UNSTABLE	UNSTABLE	UNSTABLE

BEARING PARAMETERS

D = 2.755 IN. CD′ = 0.005 IN.
L = 0.875 IN. W = 140 LB. LOAD
L/D = 0.32 EXTERNAL PRESSURE = 155 PSI

external loads on the shaft that will increase or decrease the net load on the pressure dam bearing at the coupling end. Two cases of seal and bearing load combinations were considered. In Case One, the resultant bearing load is 361 lb (the sum of the original bearing gravity load of 221 lb and 140 lb). In Case Two, the resultant bearing load is 81 lb (the difference between the original bearing gravity down-load, 221 lb, and the 140 lb seal up-load).

Figures 21 and 22 indicate the cross plots of existing coupling end pressure dam bearing coefficients for the "seal on top" and "seal on bottom" cases, respectively. With the seal on top, the pressure dam bearing coefficients increase due to the increase in load. With the seal on the bottom, the unloading effect causes the pressure dam bearing coefficients to decrease.

Figure 23 is the revised computer shaft model, which includes a third bearing at the case end seal location.

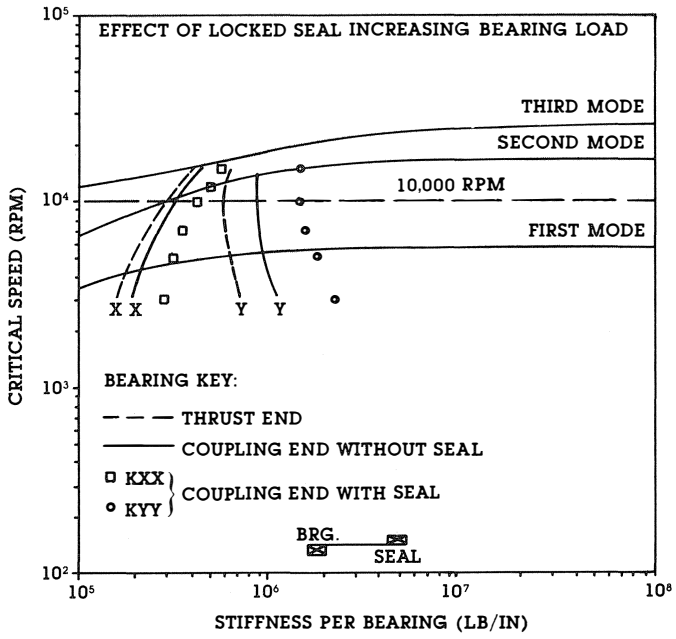

Figure 21. Critical Speed Map With Original Bearings—Locked Seal on Top.

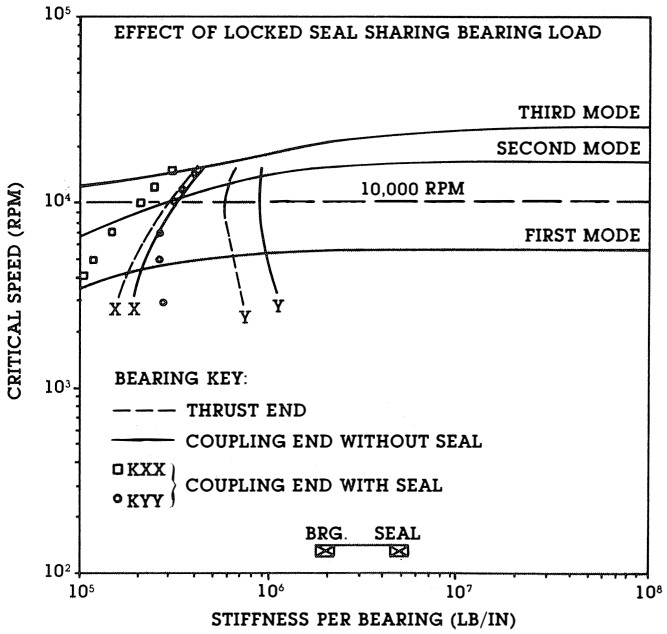

Figure 22. Critical Speed Map With Original Bearings—Locked Seal on Bottom.

Unbalance Response—Original System

A synchronous unbalance response analysis [2, 3] identifies the peak response speeds and the rotor sensitivity. The response analysis was performed for three assumed conditions: without case end seal, with locked case end seal on top (which increases the coupling bearing load), and with locked case end seal on the bottom (which decreases the coupling bearing load).

Without the case end seal, peak responses are observed in the vicinity of 3,400-3,550; 5,200-5,650; 6,550-7,300; 8,200-8,800; 11,650-11,800 and 13,000-13,600 rpm. The peak responses at 8,200-8,800 and 11,650-11,800 rpm are of particular interest, because they lie near the operating speed range of 9,000-10,000 rpm.

With the locked case end seal on top, peak responses occur at 3,700-3,850; 4,900-5,800; 11,400-11,650 and 13,000-14,500 rpm. This case shows no peaks at 8,200-8,400 rpm.

With the locked case end seal on the bottom, peaks are observed at 3,550-3,850; 4,900-5,650; 12,400-13,300; and 14,800 rpm. Again, there are no peaks at 8,200-8,400 rpm.

The overall effect of the locked case end seal on the synchronous response was very significant at the first critical speed at approximately 3,500-3,800 and 5,000-5,800 rpm. It was interesting that the bearing asymmetry produces a split critical. The peak amplitudes at the first critical show significant reductions, especially at the coupling end of the rotor.

Table 5 lists the percentage changes in predicted response amplitudes at 10,000 rpm, due to seal effects, as compared to the case without the seal. Note the extreme increase in amplitude due to the seal effect at the thrust collar, thrust end bearing, and thrust end labyrinth seal. Also, note the significant reductions of 20-70% between the rotor center and the coupling, with the exception of one case. This exception occurs at the labyrinth seal on the coupling end with case end seal on the bottom. Therefore, the case end seal significantly changes the response mode shape across the rotor by driving the amplitudes up (in very large proportions) on the thrust end and slightly reducing the coupling end amplitudes. Figures 24 through 26 illustrate this dramatic change in amplitudes between the two ends of the machine with and without the locked case end seal effect.

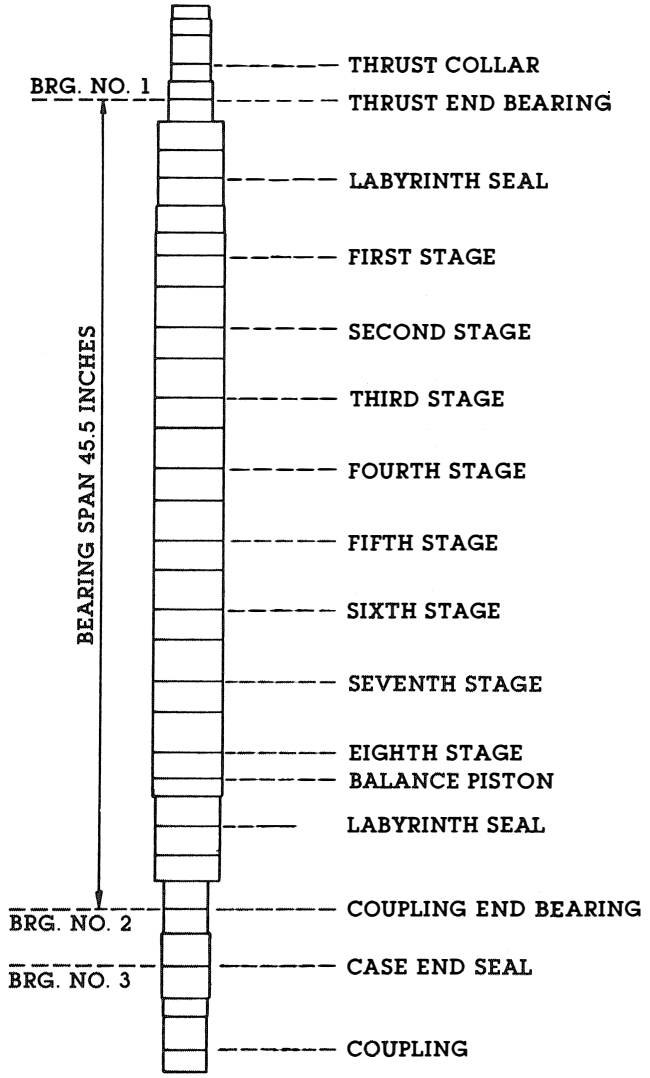

Figure 23. Revised Shaft Computer Model With Case End Seal as Third Bearing.

Table 5. Comparison of Predicted Response Amplitudes at 10,000 rpm With and Without Locked Case End Seal.

	SHAFT LOCATION							
	THRUST COLLAR	THRUST END BRG	LABY SEAL THRUST END	ROTOR CTR STAGE 5	LABY 5 AL CPLG END	COUPLING END BRG	CAS END SEAL	COUPLING
PERCENTAGE CHANGE* WITH SEAL ON TOP COMPARED TO NO SEAL								
HORIZONTAL (X)	+10,900	+5,369	+1,472	−60	−74	−69	−65	−61
VERTICAL (Y)	+ 1,043	+ 744	+ 356	−42	−69	−74	−58	−46
PERCENTAGE CHANGE* WITH SEAL ON BOTTOM COMPARED TO NO SEAL								
HORIZONTAL (X)	+ 9,157	+4,513	+1,220	−51	−74	−67	−64	−60
VERTICAL (Y)	+ 842	+ 600	+ 287	−20	+208	−65	−52	−44

*NOTE: + = INCREASE
− = DECREASE

Rotor Stability—Original System

Flexible rotor stability is assessed by calculating the system damped eigenvalues [4, 5, 6]. The damped eigenvalue ($s = \lambda + i\omega_d$) is a complex number composed of a real part (λ), which is the growth factor, and an imaginary part (ω_d), which is

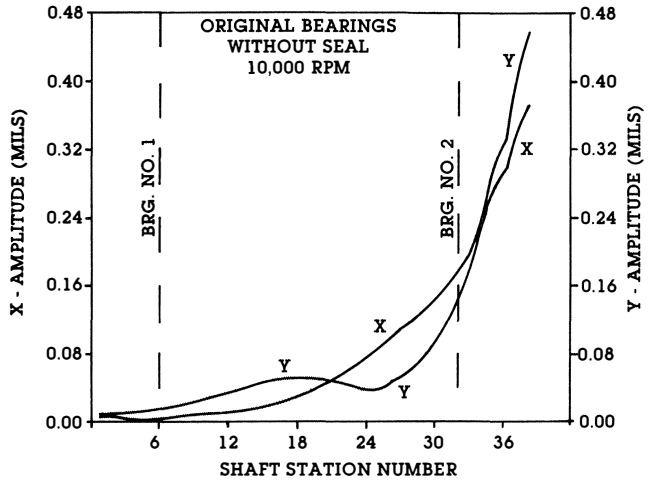

Figure 24. Predicted Rotor Amplitudes at Running Speed—Original Bearings Without Seal.

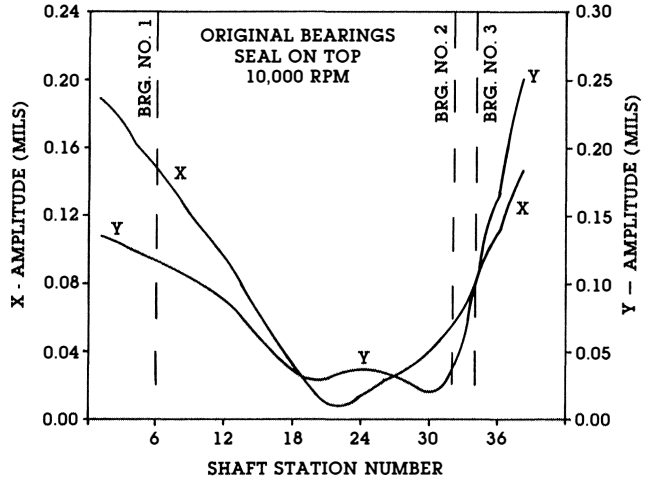

Figure 25. Predicted Rotor Amplitudes at Running Speed—Original Bearings With Seal on Top.

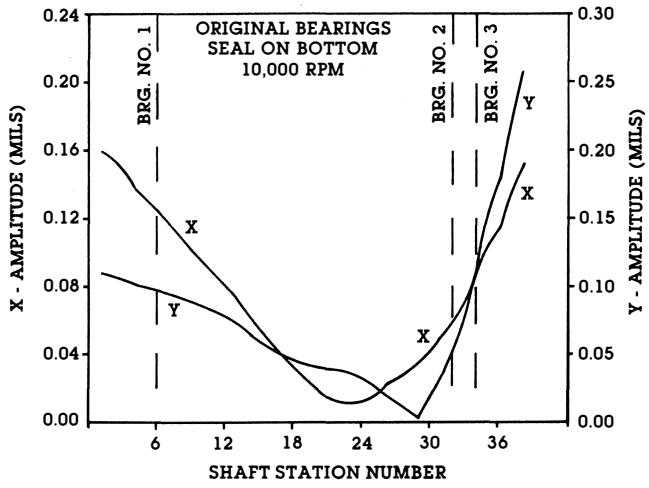

Figure 26. Predicted Rotor Amplitudes at Running Speed—Original Bearings With Seal on Bottom.

the damped frequency. The growth factor is the rate of exponential decay (or growth) of the vibration amplitudes. If λ is positive, the vibration grows with time, and the system is unstable. If λ is negative, the vibration decays with time, and the system is stable.

The log decrement (δ) is a standard non-dimensional indicator of stability of a system. It represents the natural log of the ratio of two successive amplitudes of system vibration, and it is computed from the complex eigenvalue as $\delta = -2\pi\lambda/\omega_d$. If δ is positive, the system is stable. If δ is negative, the system is unstable.

Figure 27 is a plot of log decrement versus aerodynamic cross-coupling for the original pressure dam bearings with and without the case end seal. The damped frequencies (approximately 4,100-4,200 and 5,200-5,300 rpm) correlate well with the peak response speeds at first critical (3,400-3,550 and 5,200-5,650 rpm). Figure 27 shows that the rotor system is only marginally stable. The log decrements are +0.107 with no aerodynamic cross-coupling, and +0.039 for 12,515 lb/in of aerodynamic cross-coupling. Although the rotor stability is marginal, it does not degrade dramatically with increasing destabilization. With the seal on top, the log decrements are reduced. With the seal on the bottom, the rotor is unstable under all conditions. The log decrement for this situation becomes more negative with increasing aerodynamic cross-coupling.

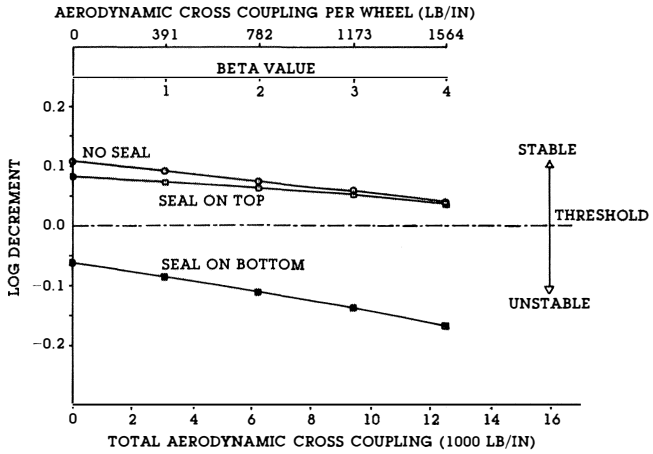

Figure 27. Flexible Rotor Stability—Original Bearings With and Without Seal.

In summary, the rotor is marginally stable with or without the case end seal effect. In fact, the case end seal reduces the stability, because it adds cross-coupling to the system. These results do not mean that the rotor will fail to operate. Instead, they are a caution that there is the possibility of whirl instability in this system. Therefore, one of the objectives of the search for new bearing alternatives was to increase the stability.

New Bearing Design

The new tilt pad bearings and process labyrinth seals are shown in Figure 28. Figure 29 shows the actual bearing and seal hardware. The bearings are five shoe tilting pad bearings with preload of 0.0 and oriented with load-between-pad. The thrust end bearing has a 2.5 in. journal diameter and 1.25 in. pad length. The coupling end bearing has a 2.5 in. journal diameter and a 1.5 in. pad length. The bearing optimization also required a heavier oil with a viscosity of 3.65×10^{-6} reyns. Figures 30 and 31 isolate the bearing components, and Figures 32 and 33 are close-ups of the new process labyrinth seals.

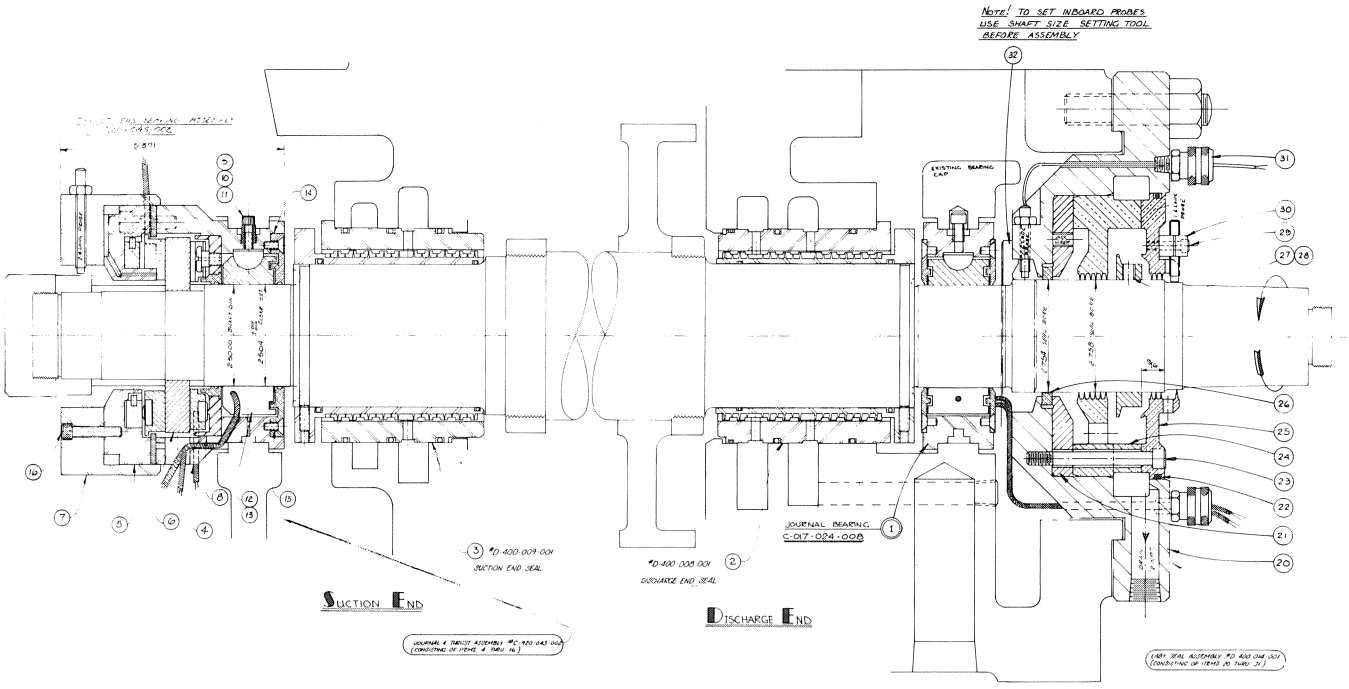

Figure 28. New Tilt Pad Bearing and Labyrinth Seal Conversion.

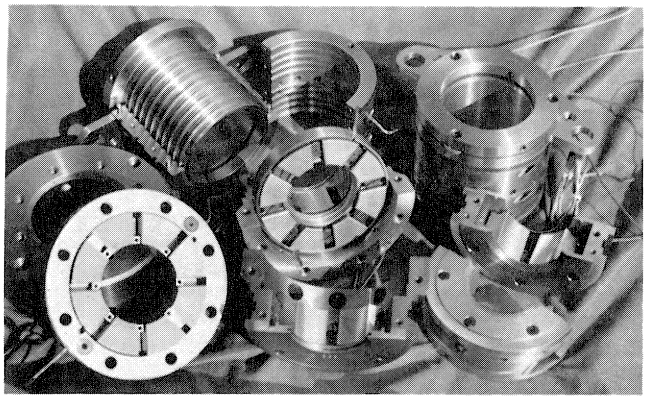

Figure 29. New Hardware—Bearings and Seals.

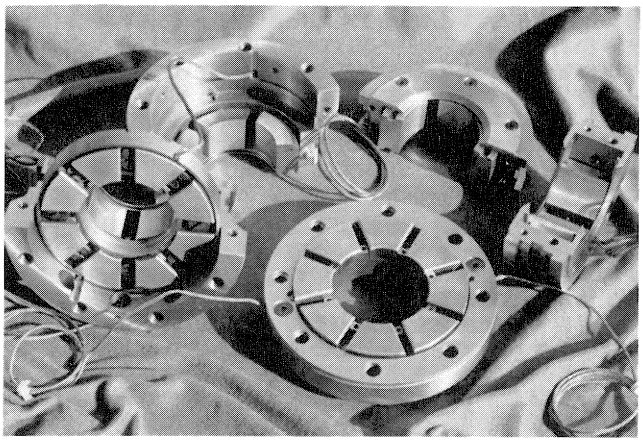

Figure 30. New Bearing Hardware.

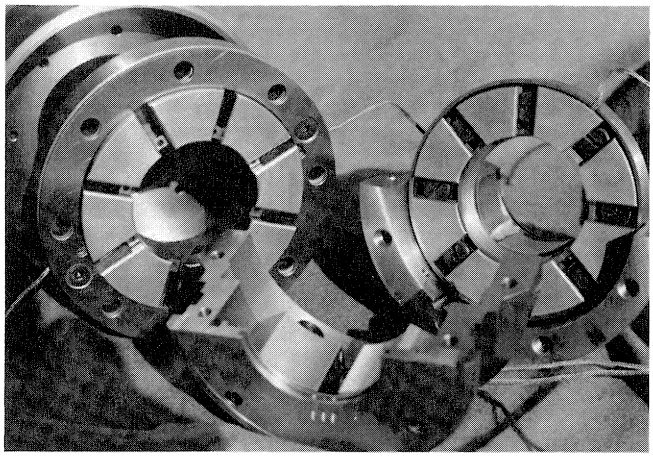

Figure 31. Close-Up of New Thrust Bearing.

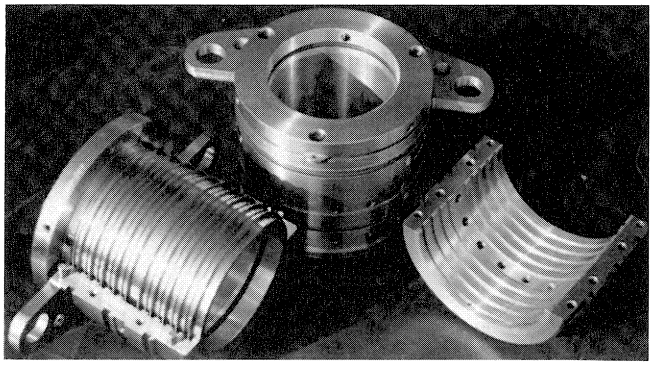

Figure 32. New Process Labyrinth Seal.

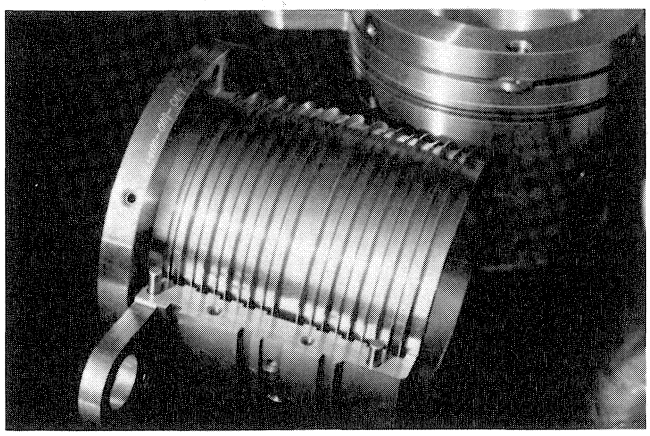

Figure 33. Close-Up of New Process Labyrinth Seal.

The stiffness coefficients for the new tilt pad bearings are shown on the critical speed map for the existing rotor in Figure 34. Table 6 lists the intersections of the new bearing stiffness and critical speed curves, which represent the undamped critical speeds with the new tilt pad bearings. The first undamped critical speeds are 3,600 and 4,200 rpm. The second undamped critical speeds are 6,000 and 7,700 rpm. The third undamped critical speeds are 11,500 and 12,000 rpm.

In order to assess the effect of different bearings on the rotor dynamics near the first critical speed, a straddle mount rotor with a relatively symmetric weight distribution can be approximated as a single mass rotor. These quantities are only approximations, based on the first mode of the rotor [7].

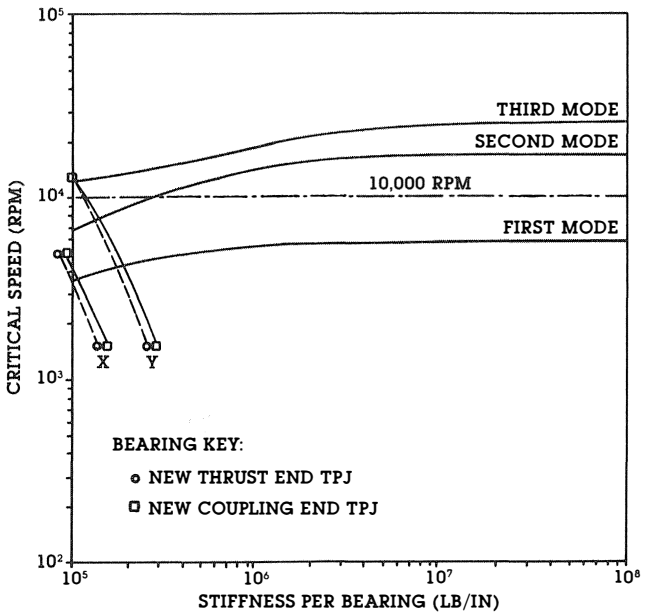

Figure 34. Critical Speed Map With New Tilt Pad Bearing Stiffness.

Table 6. Undamped Critical Speeds With New Tilt Pad Bearings.

	HORIZONTAL PLANE	VERTICAL PLANE
FIRST	3,600 RPM	4,200 RPM
SECOND	6,000 RPM	7,700 RPM
THIRD	11,500 RPM	12,000 RPM

The effective shaft stiffness can be calculated using the equation

$$K_s = \omega_{cr}^2 M_m$$

where

ω_{cr} = rigid bearing critical speed

M_m = modal mass

The total critical bearing damping can also be calculated as

$$C_{cr} = 2M_m \omega_{cr}$$

The stiffness ratio ($\bar{K}$) is the total bearing stiffness divided by the rotor stiffness. The optimum value for this ratio is 6 or less [7]. The damping ratio (ξ_{opt}) is the total actual bearing damping divided by the total critical damping. The ratio is compared to the optimum damping ratio, which is

$$\xi_{opt} = (1+\bar{K})/2$$

It should be noted that these ratios can be calculated for both the horizontal and vertical directions. However, only the vertical (Y) direction is presented here, for illustration purposes, because the gravitational rotor load causes the vertical stiffness to be higher than the horizontal stiffness.

The rotor weight for this unit is 402 lb, and the rigid bearing critical speed is 5,730 rpm. Therefore, the rotor shaft stiffness is 1.9×10^5 lb/in, and the critical bearing damping value is 625 lb-sec/in. These quantities were used to compute the stiffness and damping parameters presented in Table 7. Note that the stiffness ratio is decreased by 79% (from 8.5 to 1.8), which is well below the recommended value of 6.0. Figure 35 is a repeat of the initial critical speed map, showing both the original and new bearing stiffnesses.

Table 7. Comparison of Original and New Bearings Near Rigid Critical Speed (5,200 rpm).

TYPE	VERTICAL STIFFNESS RATIO K	ACTUAL VERTICAL DAMPING RATIO ξact	OPTIMUM VERTICAL DAMPING RATIO ξopt	% ACTUAL IS OF OPTIMUM DAMPING
ORIGINAL PRESSURE DAM	8.5	4.8	4.8	100%
NEW TILT PAD	1.8	4.2	1.4	297%
% CHANGE FROM ORIGINAL TO NEW BEARINGS	79% LOWER	13% LOWER	71% LOWER	

Table 7 also presents a comparison of actual and optimum damping ratios for the original pressure dam and new tilt pad bearings. Note that the actual damping ratio for the new bearings is 13% lower than that for the original bearings. However, the decreased stiffness causes the recommended optimum damping ratio to decrease by 71%, compared to the original case. Therefore, the new bearings have 297% of optimum, compared to 100% for the original bearings.

Unbalance Response With New Bearings

In the new tilt pad bearings, the only peak response between 1,500 and 15,000 rpm lies between 5,550 and 6,000 rpm. Therefore, there are no peaks near the continuous operating speed range (9,000-10,000 rpm) with the new bearing design.

For comparison purposes, Table 8 presents the compari-

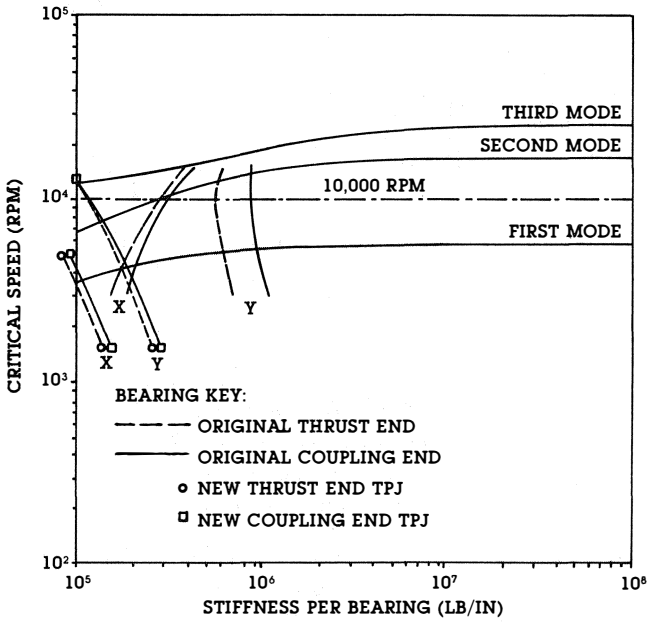

Figure 35. Critical Speed Map Comparing Original and New Bearing Stiffnesses.

Table 8. Comparison of Predicted Peak Response Amplitudes for Original and New Bearings.

	SHAFT LOCATION							
	THRUST COLLAR	THRUST END BRG	LABY SEAL THRUST END	ROTOR CTR STAGE 5	LABY SEAL CPLG END	COUPLING END BRG	CASE END SEAL	COUPLING
PRESSURE DAM BEARINGS								
1. WITHOUT SEAL % CHANGE WITH NEW TILT PAD BEARING	−77	−78	−65	−57	−55	−87	−83	−67
2. WITH SEAL ON TOP % CHANGE WITH NEW TILT PAD BEARING	−73	−75	−56	−30	−21	−62	−35	−33
3. WITH SEAL ON BOTTOM % CHANGE WITH NEW TILT PAD BEARING	−70	−72	−48	−30	−38	−62	+33	−13

son of the highest predicted peak response amplitudes at each location, over the entire speed range (up to 15,000 rpm). In all cases, the highest peak amplitudes are reduced by 13-87% with the new tilt pad bearings, except at the case end seal location, where there is a 33% increase.

Table 9 compares the amplitudes at the maximum running speed (10,000 rpm) for the new tilt pad bearings and the original pressure dam bearings. With the seal effects taken into account, the table shows amplitude reductions for the tilt pad bearings of 77-89% at the thrust collar, thrust end bearing, and thrust end labyrinth seal locations. The amplitudes at the rotor center are increased as much as 130-181%, but they still are relatively low in magnitude. The amplitudes at the coupling end labyrinth seal are reduced by 23-89%, except for one case, where there is a slight increase of 7%. Overall, the system dynamic amplitudes show a significant improvement with the new tilt pad bearings. Figure 36 is a plot of the absolute amplitudes across the shaft at maximum running speed.

Rotor Stability With New Bearings

Figure 37 is a plot of log decrement versus aerodynamic cross-coupling for the new tilt pad bearings. Remember that there is no high pressure case end seal with the new tilt pad bearing conversion. Note the significant increase in stability with the new bearings. The log decrement is +0.59 with no

Table 9. Comparison of Predicted Amplitudes at 10,000 rpm for Original and New Bearings.

	SHAFT LOCATION							
	THRUST COLLAR	THRUST END BRG	LABY SEAL THRUST END	ROTOR CTR STAGE 5	LABY SEAL CPLG END	COUPLING END BRG	CASE END SEAL	COUPLING
PERCENTAGE CHANGE FROM ORIGINAL BEARINGS WITHOUT SEAL TO NEW BEARINGS								
HORIZONTAL (X)	+1,224	+505	+155	+12	−80	−87	−72	−53
VERTICAL (Y)	+74	+15	−13	−10	−66	−84	−72	−60
PERCENTAGE CHANGE FROM ORIGINAL BEARINGS WITH SEAL ON TOP TO NEW BEARINGS								
HORIZONTAL (X)	−88	−89	−84	+181	−24	−59	−20	+21
VERTICAL (Y)	−85	−86	−81	+54	+7	−39	−33	−26
PERCENTAGE CHANGE FROM ORIGINAL BEARINGS WITH SEAL ON THE BOTTOM TO NEW BEARINGS								
HORIZONTAL (X)	−86	−87	−81	+130	−23	−61	−23	+17
VERTICAL (Y)	−82	−84	−77	+13	−89	−56	−41	−28

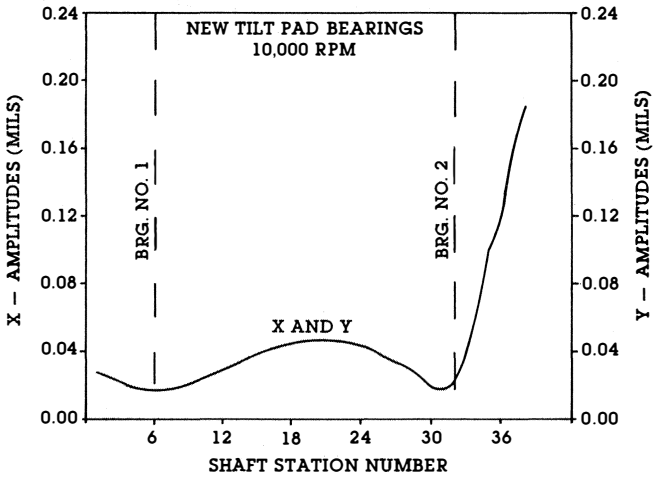

Figure 36. Predicted Rotor Amplitude at Running Speed—New Tilt Pad Bearings.

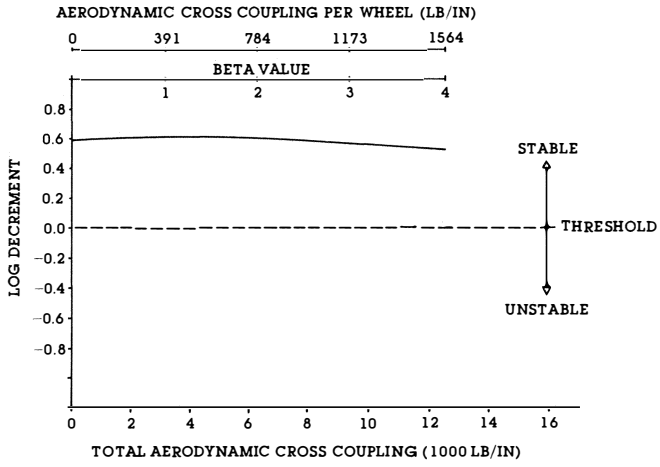

Figure 37. Flexible Rotor Stability With New Tilt Pad Bearings.

aerodynamic cross-coupling, and +0.53 with a cross-coupling value of 12,515 lb/in. Therefore, the rotor stability is excellent with the new tilt pad bearing conversion.

Conclusions From Rotor Study

1. The original rotor system with the pressure dam bearings and no case end seal had peak responses very close to running speed.

2. The locked case end seal had a very significant effect on the predicted unbalance response amplitudes at the critical speeds. These peak amplitudes showed significant reductions along the shaft between the rotor center and the coupling.
3. The locked case end seal also had a very significant effect on the predicted response amplitudes at 10,000 rpm. The seal had the effect of increasing the amplitudes on the thrust end in very large proportions and slightly settling down the coupling end.
4. The rotor stability with the original pressure dam bearings was marginal. This was true with or without the case end seal. In fact, the case end seal reduced the stability, whether it was on top or on the bottom, because it added cross-coupling to the system. These results indicated the possibility for a whirl instability in the system.
5. The optimum replacement bearings identified were five shoe tilt pad bearings with zero preload and oriented with load-between-pad. The thrust end bearing length would be 1.25 in. (L/D = 0.5), and the coupling end bearing length would be 1.5 in. (L/D = 0.6). These bearings significantly reduced the peak response amplitudes at the critical speeds and the response amplitudes at running speed (near 10,000 rpm), in comparison to the original bearing case. In addition, the rotor stability was very substantially increased with the new tilt pad bearings. The stability was marginal with the original pressure dam bearings (log decrements near zero). The log decrement with the new tilt pad bearings is in excess of +0.5, even with 12,500 lb/in of aerodynamic cross-coupling.

INSTALLATION OF NEW HARDWARE

During and after the agreement on the final design, a number of complications had to be dealt with. One of these was the 30 year old cast steel case, which could not be checked prior to the modification. This necessitated that all measurements be taken from the old case that was involved in the previous incident. Therefore, design provisions had to be made for variations between the two cases. One such problem that was not discovered until installation was the warpage of the casing that had occurred over the years. As a result, the seal bore was no longer concentric with the bearing bore.

A second complication was the tight bearing and seal space limitations that were fixed with the old case design. The new hardware had to be installed in the space allowed for the old hardware. This was a significant factor in the modified design, especially the design of the seal (refer to Figures 38 and 39). The process labyrinth seals were especially difficult to redesign, because they had to withstand pressure drops of 550 and 260 psi on the discharge and inlet ends, respectively. Recall that the original seals had much lower pressure differentials, due to the pressurized bearing housings. The drops across the original discharge and inlet seals were only on the order of 310 and 20 psi, respectively. Our commitment was to have no more leakage than could be obtained with a new compressor installation, and less if practical. The final design consisted of a labyrinth sleeve rotating in a stepped, close-clearance bore.

A third complication was that the removal of pressure from the bearing housing eliminated the need for the high pressure lube system which fed the high pressure oil seal at the coupling end of the casing. This allowed, or necessitated, the custom design of a new lube system for the new, optimized rotor-bearing arrangement. This separate lube system could accommodate the use of a higher viscosity oil, as required by the dynamic analysis. The lube system was made up with stainless steel piping and API type construction.

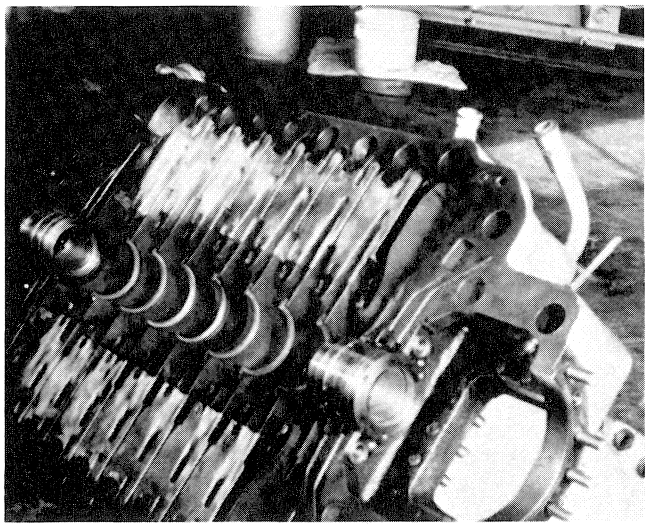

Figure 38. Upper Half of Case With New Process Labyrinth Seals Installed.

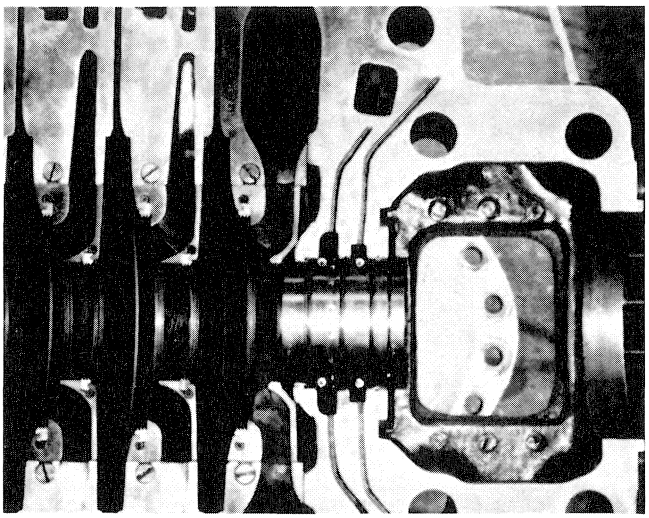

Figure 39. New Process Labyrinth Seal in Upper Half of Case—Thrust End.

The actual installation went very smoothly, with the exception of the concentricity problem between the seal and bearing bores. This necessitated the opening of the seal clearances to compensate.

The next largest problem was the flush of the oil system, which took about five days. The unit start-up was without incident.

VIBRATION ANALYSIS OF REVISED SYSTEM

The revised system is running very smoothly, with a flat, predictable transient response. Our maximum total indicated amplitudes are less than two mils. Thus, our problem now is picking the transient response data out from the "grass" (due to the low amplitudes). The vibration spectra are similar (with lower amplitudes and more repeatability) to those encountered before the conversion. However, the quality of our data has improved, since operations will now allow us to plan and set up better recordings. Figures 40 through 44 illustrate field start-up and coast-down data taken on the modified system.

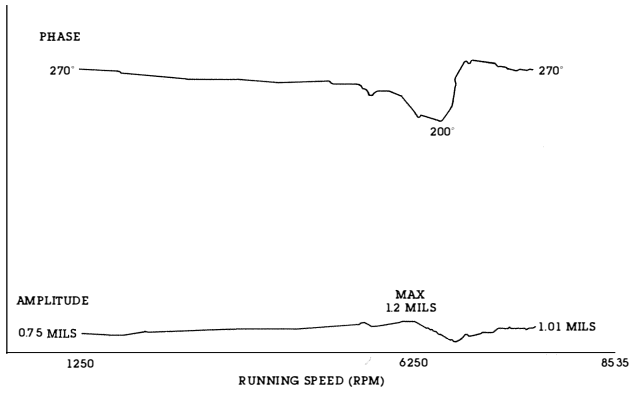

Figure 40. Post-Conversion Bode Plot—Discharge End Vertical (4/28/83 Start-Up).

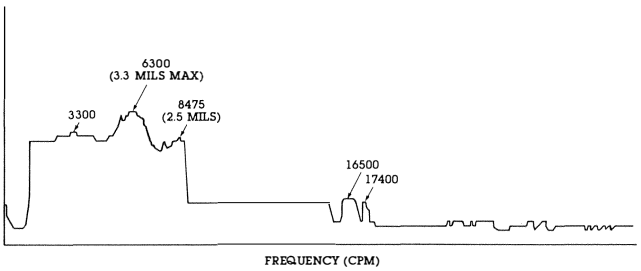

Figure 41. Post-Conversion Peak Hold Probe Amplitudes—Suction End Vertical (4/28/83 Start-Up).

Figure 40 shows a relatively flat response curve, with no pronounced amplitudes at the critical speed. The peak hold probe amplitudes at the suction end vertical are shown in Figure 41. These data indicated a major vibration peak at 6,300 rpm. The vibration increase above slow-roll is minimal. Figure 42 shows the peak hold probe amplitudes at the discharge end. The figure indicates maximum peak amplitudes of less than 1.0 mil. Figures 43 and 44 are waterfall diagrams of the modified system vibration at the discharge and suction ends, respectively. The synchronous component does not indicate any sharp responses during the coast-down. The maximum amplitudes at 8,500 rpm are 0.9 mil at the discharge end and 1.6 mils at the suction end.

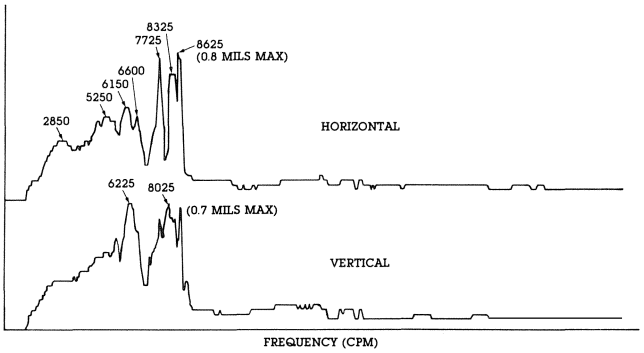

Figure 42. Post-Conversion Peak Hold Probe Amplitudes—Discharge End Vertical (4/28/83 Start-Up).

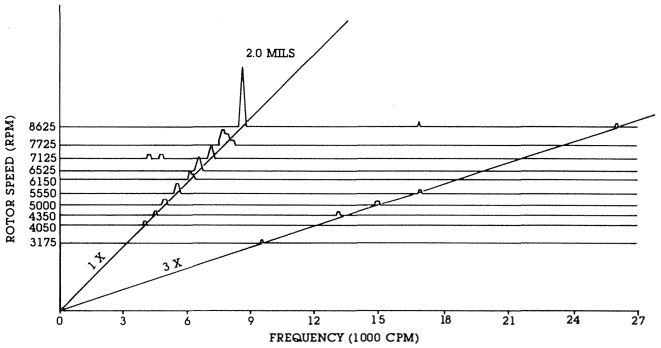

Figure 43. Post-Conversion Waterfall Diagram—Discharge End (4/10/83 Shutdown).

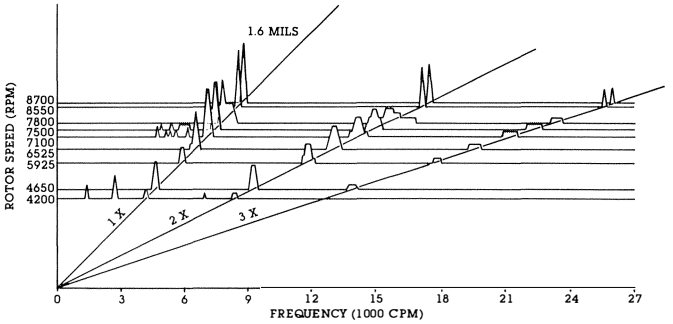

Figure 44. Post-Conversion Waterfall Diagram—Suction End (4/10/83 Shutdown).

SUMMARY

The cost of the conversion was very attractive, in that it was less than one-eighth of the estimated new compressor cost. In addition, the use of an existing compressor minimized our spare parts stocking costs and left us with a dedicated spare rotor (for this modified compressor alone). The total conversion time was less than two weeks and is estimated to have given us at least five additional production weeks over a replacement compressor installation. At this writing, the conversion has performed extremely well for fifteen months. We have had at least twelve trip-outs and six planned shutdowns of various sorts without experiencing any measurable problem. The seals allow 1¼% leakage, and they have not measurably deteriorated since the start-up. There have been no outages caused by the new bearing and seal system.

The only maintenance done so far has been routine inspections of bearings and a cleaning of the reservoir. There have been no parts replaced. The measured vibration is uniformly low, with very low critical speed amplitudes. We are pleased with the performance of the modified system.

REFERENCES

1. Nicholas, J. C. and Allaire, P. E., "Analysis of Step Journal Bearings—Finite Length, Stability," Trans. ASLE, *23*, 2, pp. 197-207 (1980).
2. Lund, J. W. and Orcutt, F. K., "Calculations and Experiments on the Unbalance Response of a Flexible Rotor," Journal of Engineering for Industry, Trans. ASME, Series B, *89*, 4, pp. 785-796 (1967).
3. Salamone, D. J. and Gunter, E. J., "Effects of Shaft Warp and Disk Skew on the Synchronous Unbalance Response of a Multimass Flexible Rotor in Fluid Film Bearings," In *Topics in Fluid Film Bearing and Rotor Bearing System Design and Optimization*, ASME Book No. 100118 (1978).

4. Gunter, E. J., *Dynamic Stability of Rotor-Bearing Systems*, NASA SP-113, Office of Technical Utilization, U.S. Government Printing Office, Washington, DC (1966).

5. Lund, J. W., "Stability and Damped Critical Speeds of a Flexible Rotor in Fluid Bearings," Journal of Engineering for Industry, Trans. ASME, Series B, *96*, 2, pp. 509-517 (1974).

6. Gunter, E. J. and Trumpler, P. R., "The Influence of Internal Friction on the Stability of High Speed Rotors with Anisotropic Supports," Journal of Engineering for Industry, Trans. ASME, Series B, *91*, 4, pp. 1105-1128 (1969).

7. Barrett, L. E., Gunter, E. J. and Allaire, P. E., "Optimum Bearing and Support Damping for Unbalance Response and Stability of Rotating Machinery," Journal of Engineering for Power, Trans. ASME, *100*, 1, pp. 89-94 (1978).

ACKNOWLEDGEMENT

The authors would like to acknowledge Mr. Ken Sutton, Senior Maintenance Engineer of Celanese, for his assistance in the successful execution of this project, especially during the installation and start-up phase.